Biochemical and Biophysical Research Communications 428 (2012) 127–131

Contents lists available at SciVerse ScienceDirect

Biochemical and Biophysical Research Communications

journal homepage: www.elsevier.com/locate/ybbrc

Changes in the dielectric properties of medaka fish embryos during development, studied by electrorotation

Ryo Shirakashi [a,*], Miriam Mischke [b], Peter Fischer [c], Simon Memmel [b], Georg Krohne [d], Günter R. Fuhr [e], Heiko Zimmermann [f], Vladimir L. Sukhorukov [b,*]

[a] Institute of Industrial Science, The University of Tokyo, Tokyo 153-8505, Japan
[b] Lehrstuhl für Biotechnologie und Biophysik, Biozentrum, Universität Würzburg, Würzburg, Germany
[c] Physiologische Chemie, Biozentrum, Universität Würzburg, Würzburg, Germany
[d] Abteilung für Elektronenmikroskopie, Biozentrum, Universität Würzburg, Würzburg, Germany
[e] Lehrstuhl für Biotechnologie und Medizintechnik, Universität des Saarlandes, Saarbrücken, Germany
[f] Lehrstuhl für Molekulare und Zelluläre Biotechnologie, Universität des Saarlandes, Saarbrücken, Germany

ARTICLE INFO

Article history:
Received 25 September 2012
Available online 11 October 2012

Keywords:
Oryzias latipes
Dielectric spectroscopy
Permittivity
Conductivity
Chorion
Yolk membrane
Hanging droplet

ABSTRACT

The Japanese medaka fish, *Oryzias latipes*, has become a powerful vertebrate model organism in developmental biology and genetics. The present study explores the dielectric properties of medaka embryos during pre-hatching development by means of the electrorotation (ROT) technique. Due to their layered structure, medaka eggs exhibited up to three ROT peaks in the kHz–MHz frequency range. During development from blastula to early somite stage, ROT spectra varied only slightly. But as the embryo progressed to the late-somite stage, the ROT peaks underwent significant changes in frequency and amplitude. Using morphological data obtained by light and electron microscopy, we analyzed the ROT spectra with a three-shell dielectric model that accounted for the major embryonic compartments. The analysis yielded a very high value for the ionic conductivity of the egg shell (chorion), which was confirmed by independent osmotic experiments. A relatively low capacitance of the yolk envelope was consistent with its double-membrane structure revealed by transmission electron microscopy. Yolk-free dead eggs exhibited only one co-field ROT peak, shifted markedly to lower frequencies with respect to the corresponding peak of live embryos. The dielectric data may be useful for monitoring the development and changes in fish embryos' viability/conditions in basic research and industrial aquaculture.

1. Introduction

Fish models, such as Japanese medaka, are widely used in genetic, developmental and biomedical studies as an alternative to mammals, due to their easy availability, low maintenance cost, external embryo development, and many other advantages [1–3]. Medaka is a small, egg-lying freshwater fish, found primarily in Japan. Its embryogenesis and genetics have been extensively studied during past decades [4,5]. According to [6], the pre-hatching development of medaka embryos can be divided morphologically into 39 stages.

Transparent, medaka eggs are highly suitable for studies of fish embryogenesis using combined morphological and biophysical approaches [7,8]. Shortly after fertilization, massive changes in the electrical properties of medaka oocytes have been detected by means of electrophysiological techniques [7,9]. Particularly, the capacitance of the egg membrane transiently doubles and its conductance increases even 10-fold within few minutes after fertilization [9].

Taking advantage of a non-invasive, electrical impedance technique, Asami et al. succeeded in long-term and real-time monitoring of the development of medaka eggs by their dielectric behavior over the kHz–MHz frequency range [10]. In that study, the impedance spectra of single medaka embryos have been measured continuously for up to 6 days of development. The impedance spectra have exhibited a strong Debye-type dielectric dispersion caused by a Maxwell–Wagner relaxation occurring, most likely, at the outer interface of the yolk membrane.

A deeper insight into the dielectric structure of medaka embryos might be gained by studying their electromechanical response to rotating electric fields. In the last years, the electrorotation (ROT) and related electrokinetic techniques have become the principal means for the dielectric characterization and manipulation of biological cells [11–15]. ROT offers several advantages over impedance measurements, such as improved frequency resolution, no influence of electrode polarization, simpler modeling, etc. [16,17].

* Corresponding author.
E-mail addresses: aa21150@iis.u-tokyo.ac.jp (R. Shirakashi), sukhorukov@biozentrum.uni-wuerzburg.de (V.L. Sukhorukov).

0006-291X/$ - see front matter © 2012 Elsevier Inc. All rights reserved.
http://dx.doi.org/10.1016/j.bbrc.2012.10.019

Although, the ROT technique poses no limitations to the cell size, most ROT studies published so far have been restricted to relatively small-sized biological cells with a diameter of up to 100 μm [18–20]. There is only one report available on the ROT of the much larger axolotl embryos, measuring ~2 mm in diameter [21]. In fact, electrorotation of the non-buoyant, mm-sized medaka eggs in conventional ROT chambers was hardly possible, mainly because of a high friction between the egg and the chamber floor. We overcome this problem by rotating freely suspended fish eggs, which were entrapped by surface tension within a hanging droplet. The integration of the ROT and hanging-droplet techniques allowed us to conduct accurate ROT measurements on medaka eggs during development between stages ~10 and ~30. Analysis of the ROT spectra with a three-shell model yielded the dielectric parameters of the major structural units of fish eggs.

2. Materials and methods

2.1. Fish

Populations of medaka were maintained in freshwater at 24–26 °C under a natural (Tokyo) or artificial photoperiod of 14-h light to 10-h darkness (Würzburg). Naturally fertilized eggs were collected after natural spawning. Long attaching filaments were cut off to facilitate ROT.

2.2. Electrorotation

The ROT chamber was arranged as an array of eight rectangular electrodes manufactured on quartz glass (Pyrex 7740) by electroplating gold to a thickness of ~1 μm, as described previously [11,16]. The distance between two opposite electrodes was 1 mm. The electrodes were short-circuited in pairs and driven by four 90° phase-shifted rectangular signals from a ROT-field generator with 15 V_{PP} amplitude. ROT spectra were monitored by decreasing the field frequency from 20 MHz to ~100 Hz, in 4 steps percent decade (see Supplemental videos).

ROT spectra were measured at different external conductivities, which were adjusted by mixing appropriate amounts of deionized water (6 μS/m) from a Milli-Q water purification system (Millipore, Tokyo, Japan) with Tokyo tap water (~20 mS/m). Conductivity was measured by means of a conductometer B-173 (Horiba, Kyoto, Japan). For electrorotation, 50 μL of suspending medium was pipetted centrally onto the ROT chamber to form a near semi-spherical droplet. An egg was collected with forceps and dipped into the droplet. The chamber was then gently turned upside-down to allow the egg to slide by gravity at the air–water interface down to the apex of the *hanging droplet* (Supplementary Fig. S1). Egg's ROT was observed using an inverted microscope (CK2, Olympus, Tokyo, Japan) equipped with a low magnification 2× objective. The ROT spectra were recorded using a camcorder (HDR-SR1, Sony, Tokyo, Japan) for later analysis.

2.3. Electron microscopy

Transmission electron microscopy (TEM) served to determine the thickness of the chorion and to examine the yolk envelope in the early-stage medaka embryos. Sample preparation and TEM measurements are described in detail in the Supplementary material (Part 2).

3. Results and discussion

Embryos at the Iwamatsu stages 9–11 [6], denoted as early-stage eggs, were the earliest available stages for these experiments. Embryos at stages ~20 and ~30 are referred to as mid and late-stage eggs, respectively.

3.1. Changes in the ROT spectra during development

Depending on the external conductivity the ROT spectra of *live* embryos exhibited 2 or 3 peaks, including anti- and co-field peaks at low- and high-frequencies (LF and HF, Fig. 1). A double or triple Lorentzian function (Eq. S7) matched very well the ROT spectra, yielding the values for the characteristic frequencies ($f_{c1,2,3}$) and magnitudes of the ROT peaks (see Table S1).

The ROT spectra of early-stage embryos shown in Fig. 1A revealed a strong effect of external conductivity (σ_e) on the position and magnitude of the LF anti-field peak (f_{c1}/A_1). Upon increasing σ_e from 1 to 11 mS/m the f_{c1} peak shifted gradually from ~3 to ~6.6 kHz, and its magnitude (A_1) increased steadily from ~0.02 to ~0.07 rps (Table S1). At the lowest conductivity of ~1 mS/m, a minor co-field peak in the sub-MHz range ($f_{c2} \approx 0.35$ MHz, $A_2 \approx 0.02$ rps) appeared in the spectrum, whereas at higher conductivities (5–11 mS/m) the ROT spectra did not show any appreciable peaks in this frequency range. Frequencies above 10 MHz gave rise

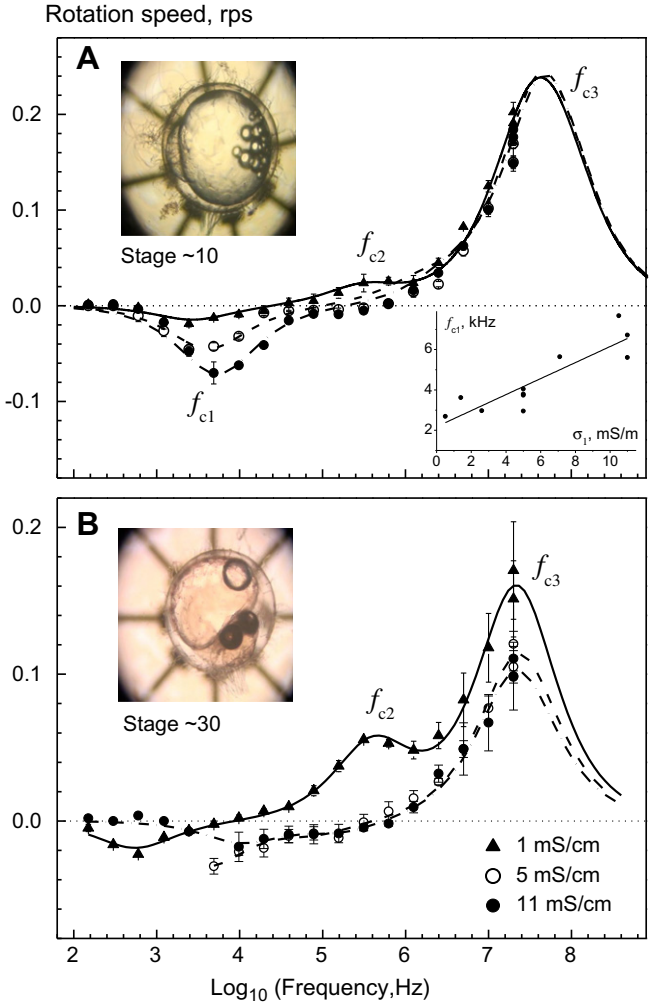

Fig. 1. ROT spectra of live medaka embryos in the development stages ~10 (A) and ~30 (B), measured at the indicated external conductivities. Each spectrum (*symbols*) is the mean (±SE) of 3–5 independent measurements. Curves in (A) are best fits of the three-shell model (TSM, Eqs. S5 and S6). The best-fit parameters derived with the TSM are given in Table 1. In (B), best Lorentzian fits (Eq. S7, in B) are shown. The RHS inset in (A) shows the conductivity dependence of the characteristic frequency f_{c1}. For details see text.

to the major co-field peak, whose characteristic frequency (f_{c3}) was not reached in our experiments. Nevertheless, both position and magnitude of this peak (f_{c3}/A_3) could be estimated very accurately from the Lorentzian fits (Table S1). Unlike the anti-field ROT peak (f_{c1}/A_1), the major co-field showed quite constant $f_{c3} \approx 30$ MHz and $A_3 \approx 0.2$ rps over the whole conductivity range. The ROT spectra of mid-stage embryos were similar to those of early-stage eggs (Table S1), which corroborates the finding that the impedance spectra do not change significantly between early and mid-stages of development [10].

The ROT spectra changed markedly as the embryos progressed from to late-stage (Fig. 2B). Hereby the major co-field peak shifted slightly to lower frequency ($f_{c3} \approx 20$ MHz) and its magnitude decreased by 25–50%. The magnitude of the intermediate peak (f_{c2}) increased from 0.014–0.02 rps (early and mid-stages) to 0.05 rps in the ROT spectrum of late-stage embryos.

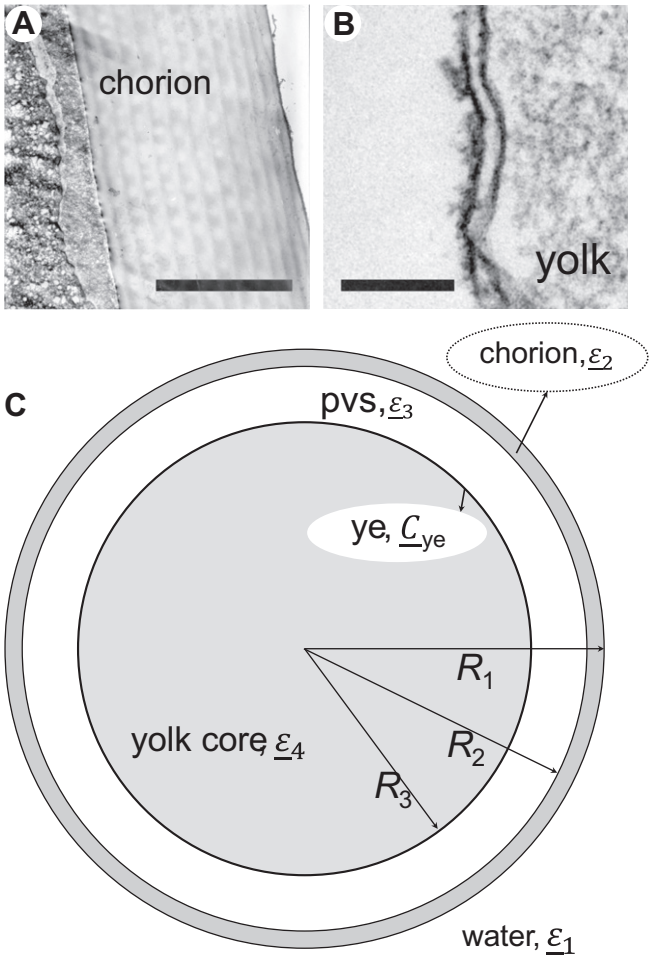

Fig. 2. Electron micrographs (TEM) of cross-sectioned early-stage medaka eggs illustrating the chorion (A; bar = 10 μm) and the yolk envelope (B; bar = 100 nm). The chorion is 15 μm thick and exhibits a characteristic "tree-ring"-like structure. Part (B) reveals the double-membrane structure of the yolk envelope. The two parallel electron-dense layers in (B), corresponding to the inner and outer yolk membranes, are separated by the electron lucent rim of cytoplasm with a thickness of ~15 nm. Part (C) illustrates a three-shelled dielectric sphere as a structural model of an early-stage medaka embryo. Beginning from the outside, the concentric shells are the chorion, perivitelline space (pvs) and yolk envelope (ye). R_1, R_2 and R_3 are the radii of the corresponding boundaries. The external radius of the chorion $R_1 = 600$ μm, its thickness $R_1 - R_2 = 15$ μm, and the thickness of pvs $R_2 - R_3 = 50$ μm were determined from the microphotographs, such as shown in Part (A) and Fig. S2. In the model, the embryo's layers and the surrounding aqueous medium are viewed as lossy dielectrics having complex permittivities ε's or capacitance C_{ye}. Subscripts 1, 2, 3, ye and 4 denote the external medium, chorion, pvs, yolk envelope, and yolk core, respectively. For further detail see Supplementary data and Table 1.

3.2. The three-shell dielectric model of an early-stage medaka embryo

Previous histologic and electron microscopic studies revealed a complex multilayered structure of medaka eggs, common to teleost fishes [22]. Medaka eggs and early stage embryos are nearly perfect spheres measuring uniformly 1.2 mm in diameter [6]. Teleost eggs contain at least two distinct envelopes: the outer chorion capsule and the inner vitelline membrane (yolk envelope), which surrounds a large yolk sphere (see Figs. S2A–2C).

The chorion forms the hard outer shell of fish eggs. The thickness of the chorion during the early- and mid-stages of medaka development remains constant at 15 μm [22], which perfectly agrees with our TEM data (Fig. 2A).

Between the chorion and the yolk, there is a ~50 μm-wide perivitelline space (pvs) filled with an aqueous solution of polysaccharides [6]. With a radius $R_3 = 0.55$ mm, the membrane-bound yolk sphere forms the largest compartment (~80% in volume) of medaka eggs. The complex morphology of medaka eggs calls for a multi-shelled dielectric model (Fig. 2C). Given that up to a stage ~20 the embryoblast occupies only a small volume fraction of the whole egg (see Figs. S2A–S2D), a triple-shelled sphere appears to provide a reasonable model for early- or mid-stage medaka embryos.

3.3. Derivation of dielectric properties of early-stage medaka eggs

The mathematical expression for the ROT speed of a triple-shelled particle (Eqs. S5 and S6 in Supplementary data) contains 15 parameters, including 3 geometric ($R_{1,2,3}$) and 10 dielectric quantities, as well as the effective local field strength E_0 and the viscosity of suspending medium η. The geometric data were determined from the light and electron microphotographs or found in the literature (Table 1). The conductivity σ_1 (1–11 mS/m), permittivity ($78\varepsilon_0$) and viscosity $\eta \approx 1$ mPa s of the aqueous suspending medium were measured independently (σ_1) or taken from the literature. The permittivity of the aqueous perivitelline space can also be assumed as that of water ($\varepsilon_3 = 78\varepsilon_0$). Since the ROT spectra measured at kHz–MHz frequencies might be poorly sensitive to the *direct-current* conductance G_{ye} of the yolk envelope, we used in the following calculations a G_{ye} value of 0.15 S/m^2, corresponding to the mid resistance within the range 50–100 kΩ cm^2 reported in [10].

We are still left with seven unknown parameters, including σ_2, ε_2, σ_2, C_{ye}, σ_4, ε_4, and the scaling factor (*sf*, defined by Eq. S6), whose symbols and dimensions are given in Table 1. To estimate the unknown quantities we tried to fit the TSM (Eqs. S5 and S6) to the experimental ROT spectra. Prior to least-square calculations, we determined the starting values for several unknown parameters using the experimental f_c data (Table S1) and approximate equations for ROT peak frequencies available in the literature [13,16,17].

Thin membrane-like structures, e.g. yolk envelope and chorion, might be capacitively bridged at frequencies >1 MHz. Therefore, the polarization of the yolk core should dominate the major co-field peak of early-stage eggs. Using the f_{c3} data obtained by Lorentzian fits (Table S1), we can roughly assess the conductivity σ_4 of the yolk core by applying Eq. S9. The substitution of $f_{c3} = 26$–32 MHz (Table S1), $\varepsilon_4 = \varepsilon_1 = 78$ and $\sigma_1 \approx 11$ mS/m into this equation yields a σ_4 range of 0.34–0.42 S/m.

The conductivity-dependence of the anti-field peak (f_{c1}) of early-stage eggs (Fig. 1A) is typical for a membrane charging process [18,20,23]. An early-stage medaka egg has two membranous structures: the 15 μm-thin chorion capsule and the yolk envelope. To find out whether the chorion or the yolk envelope gave rise to the anti-field peak, we analyzed the f_{c1}-data with Eq. S8, derived on the basis of a single-shell model (SSM). Linear regression of Eq. S8 to the f_{c1} data plotted *vs* σ_1 in the inset of Fig. 1A yielded

Table 1
Dielectric and geometric parameters used for calculations of the ROT spectra of the early-stage medaka embryos on the basis of the three-shell model (TSM).

Parameters	Symbol	Known parameters	Derived quantities
External conductivity (variable)	σ_1	1, 5, 11 mS/m	
External permittivity	$\varepsilon_1\varepsilon_0$	$78\varepsilon_0$	
Scaling factor	$sf = \varepsilon_1\varepsilon_0 E_0^2/2\eta$		0.54
The outer radius of the egg	R_1	600 μm	
Chorion thickness	$R_1 - R_2$	15 μm	
Chorion conductivity	σ		$\sim 0.5\sigma_1$
Chorion permittivity	$\varepsilon_2\varepsilon_0$		$\sim 30\varepsilon_0$
Thickness of the perivitelline space, pvs	$R_2 - R_3$	50 μm	
pvs conductivity	σ_3		$0.3 + 30\sigma_1$ S/m
pvs permittivity	$\varepsilon_3\varepsilon_0$	$78\varepsilon_0$	
Yolk radius	R_3	550 μm	
Conductance of the yolk envelope	G_{ye}	0.2 S/m^2	
Capacitance of the yolk envelope	C_{ye}		4–5 mF/m^2
Conductivity of the yolk core	σ_4		0.35–0.40 S/m
Permittivity of the yolk core	$\varepsilon_4\varepsilon_0$		$\sim 60\varepsilon_0$

a C_{SSM} = 1.34 ± 0.23 mF/m^2. The substitution of this C_{SSM} value and the chorion thickness d_{ch} = 15 μm into the relation $C = \varepsilon_{rel}\varepsilon_0/d$ gives a very high value of $\varepsilon_{rel} = 2.3 \times 10^3$ for the relative chorion permittivity, unusual for most dielectric materials. Particularly, the relative dielectric constant of proteins, e.g. ~20 [24], is ~two orders of magnitude lower than the calculated one. Given that the chorion is composed of glycoproteins [6], it was definitely not responsible for the LF antifield peak. Consequently the f_{c1}-peak can be attributed to the yolk envelope.

To derive the unknown parameters, we fitted the TSM (Eqs. S5 and S6) to the ROT spectra using the nonlinear least-square package of Mathematica. The fitting procedure included two steps. In the first step, involving 2D-curve fitting, individual ROT spectra were consecutively fitted to the TSM-based function $\Omega(f)$ containing the field frequency as the single variable. In the second step (3D-surface fitting), all available ROT spectra measured over the conductivity range $1<\sigma_1<11$ mS/cm were *simultaneously* fitted to the TSM presented as a function of two variables $\Omega(f,\sigma_1)$. A two-step procedure was necessary because of a strong dependence of the chorion and pvs conductivities on the external conductivity σ_1. Analysis of the σ_2 and σ_3 values obtained by 2D-fitting led to the following linear relationships: $\sigma_2 = 0.5\sigma_1$ and $\sigma_3 = 0.3 + 30\sigma_1$. Using these assumptions, the simultaneous 3D-surface fit yielded best-fit values for the scaling factor *sf*, ε_2, C_{ym}, σ_4 and ε_4, summarized in Table 1.

3.4. Validity of the fitted parameters

The TSM-based analysis yielded a C_{ye} value of 4–5 mF/m^2 for the area-specific capacitance of the yolk envelope, which is exactly half of the 8–10 mF/m^2 reported for the capacitance of mammalian cells [14–16]. At the same time, the low C_{ye} obtained here is typical for two serially arranged membranes, such as the plasmalemma and vacuolar membrane of plant cells [18,20]. In agreement with our data, earlier electrophysiological studies also suggest that the yolk envelope of fish eggs may consist of two lipid bilayers, including the internal and external yolk membranes [7]. In medaka eggs, the two yolk membranes might be separated by a rather thin cytoplasmic layer, which could not be resolved by light microscopy.

In order to prove the presence of a double yolk membrane, we analyzed the yolk boundary by transmission electron microscopy (TEM). In fact, electron micrographs of cross-sectioned medaka eggs taken under a high magnification of 25,000 × clearly reveal the double-membrane structure of the yolk envelope (Fig. 2B). The two membranes are separated by only ~10–15 nm or even attached to each other. Accordingly, the equivalent electrical circuit of the yolk envelope should strictly include two serially connected capacitances. In view of the close vicinity of both membranes (Fig. 2B), the three-shell model used here (Fig. 2C) treats the yolk envelope as a single homogeneous layer, whose effective capacitance C_{ye} = 4–5 mF/m^2 is composed of the internal and external yolk membranes arranged in series. Otherwise, a five-shell model with further six parameters would be necessary.

The TSM-based analysis also showed that the chorion and pvs conductivities increased linearly with the external conductivity σ_1 (Table 1). This finding implies a substantial permeability of the chorion for electrolytes. To prove this result we analyzed the permeation of various solutes through the chorion of early-stage medaka eggs under hypertonic conditions (Supplementary data). As suggested by their osmotic action on medaka eggs (Fig. S4), the tested solutes can be divided into two groups. Small inorganic ions, i.e. Na^+ and Cl^-, and small-sized PEG200–300 were capable of permeating the chorion. In contrast, the chorion was fully impermeable for PEG400 and larger. The high osmotic permeability of the chorion for inorganic ions corroborates its high electric conductivity derived from the ROT spectra.

3.5. Rotation of dead/undeveloped eggs

The ROT spectra of dead/undeveloped eggs (Fig. 3) were completely different from those of live embryos (Fig. 1). The difference can be attributed to a less complex dielectric structure of the yolk-free dead eggs, consisting only of an empty chorion capsule (inset in Fig. 3). Given the single-shell structure of dead eggs, two peaks can be expected in their ROT spectra, arising from the charge relaxations at the inner and outer boundaries of the chorion. In practice, however, the ROT spectra of dead eggs exhibited only one co-field peak over the whole conductivity range (Fig. 3).

Centered between ~5 and ~8 MHz, the cofield peak of dead eggs was shifted by ~one decade to lower frequency with respect to the corresponding f_{c3} peak of live embryos ~20–50 MHz. Analysis with the single-shell model (not shown) revealed that the main peak in the ROT spectra of dead eggs was due to the polarization of the intrachorionic fluid. At the same time, the absence of the sec-

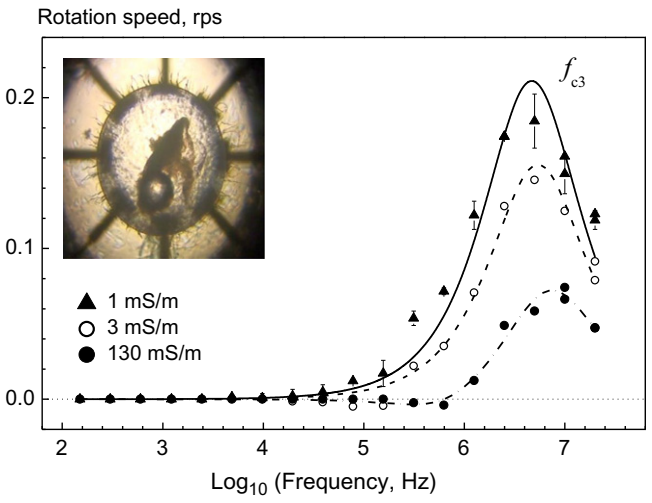

Fig. 3. ROT spectra of dead medaka embryos at various conductivities of suspending medium. Unlike live embryos, the yolk-free dead eggs exhibited only one co-field peak, shifted by almost one decade to lower frequencies with respect to the corresponding f_{c3} peak of the early stage live embryos (Fig. 1A).

ond peak, expected theoretically for single-shelled particles, can be explained by a high conductivity of the chorion. The latter conclusion is consistent with the data for live medaka embryos discussed above. By applying Eq. S9 and using the f_{c3} data (Table S1), we also found that the conductivity of intrachorionic fluid in dead eggs (σ_i = 62–82 mS/m) was much smaller than the conductivity of the yolk core σ_4 = 400 mS/m in live eggs.

3.6. Dielectric mechanisms underlying the ROT spectra of live peaks

The lack of anti-field peak in the spectra of *yolk-free* dead embryos (Fig. 3) is clear evidence that the anti-field peak f_{c1} centered at ~10 kHz in the ROT spectra of live embryos was dominated by the capacitive charging of the yolk envelope. This conclusion was also confirmed by the numerical simulations with the TSM illustrated in Fig. S3 (Supplementary data). As seen in Fig. S3B, increasing the conductivity of yolk envelope, e.g. via its permeabilization or rupture by membrane-lytic agents or other mechanisms, would lead to a progressive reduction and disappearance of the anti-field peak. Accordingly, the anti-field ROT at frequencies below 100 kHz may serve as a sensitive indicator for the integrity of the yolk envelope in viable medaka eggs during early developmental stages.

A further useful indicator of fish embryos with an intact yolk is the major co-field ROT peak centered at frequencies above ~10 MHz (f_{c3} in Fig. 1). Our analysis with the TSM showed that this peak resulted mainly from the polarization of the yolk core. The numerical simulations in Fig. S3C illustrate additionally the strong dependence of the f_{c3} peak on the yolk core conductivity. Our ROT experiments showed that the yolk core peak did not change much between stages ~10 and 20 (Table S1), but it decreased considerably in magnitude as the embryo reached stage ~30 (Fig. 1B). This result corroborates the earlier morphological findings that the yolk in medaka eggs remains constant in volume up to stage ~25, but after that, the yolk volume decreases steeply from the initial 0.7 μL to ~0.3 μL at 7 day post-fertilization [25].

The remaining minor co-field peak centered at $f_{c2} \approx 0.4$ MHz was detected in the ROT spectra of early-stage embryos only at the lowest external conductivity (Fig. 1A). The weak contribution of the chorion to the ROT spectrum can be explained by the very high ionic permeability/conductivity of this porous polypeptide shell discussed above. Computations with the TSM showed that the f_{c2} peak was very sensitive to the permittivity of the chorion ε_2, as illustrated in Fig. S3D. Accordingly, the strongly increased magnitude of this peak during late pre-hatching stages (Fig. 1B) may have been caused by a decrease in permittivity of the chorion resulted probably from impregnation of this porous layer with oily substances released from the yolk, such as the numerous oil drops seen in Figs. S2A–S2C.

In conclusion, the electrorotation technique has proved a powerful non-invasive tool for the analysis of dielectric properties of fish eggs/embryos during development. Although this study focuses on the Japanese medaka, the approach presented here can be generally applied for the analysis of other extra-large biological cells and particles, measuring 1–2 mm in diameter. The biophysical data presented here are of interest not only for developmental biology but also for biotechnology and aquaculture, were dielectric techniques are widely used for monitoring the quality, conditions and viability of fish eggs and fries during pre-hatching stages.

Acknowledgments

We thank Mrs. C. Gehrig and Mrs. D. Bunsen (University of Würzburg) for expert assistance with electron microscopy. We are grateful to Mr. M. Uemura (University of Tokyo) for providing us with medaka eggs. We also thank Prof. M. Schartl (University of Würzburg) for discussions and critical reading of the manuscript. V.L.S. was supported by an Invitation Fellowship Programs for Research at IIS, the University of Tokyo.

Appendix A. Supplementary data

Supplementary data associated with this article can be found, in the online version, at http://dx.doi.org/10.1016/j.bbrc.2012.10.019.

References

[1] S.R. Porazinski, H. Wang, M. Furutani-Seiki, Essential techniques for introducing medaka to a zebrafish laboratory – towards the combined use of medaka and zebrafish for further genetic dissection of the function of the vertebrate genome, Methods Mol. Biol. 770 (2011) 211–241.
[2] T. Okuyama, Y. Suehiro, H. Imada, A. Shimada, K. Naruse, H. Takeda, Induction of c-fos transcription in the medaka brain (*Oryzias latipes*) in response to mating stimuli, Biochem. Biophys. Res. Commun. 404 (2011) 453–457.
[3] Y. Isoe, T. Okuyama, Y. Taniguchi, T. Kubo, H. Takeuchi, Mutation suppresses adult neurogenesis in medaka fish (*Oryzias latipes*), Biochem. Biophys. Res. Commun. 423 (2012) 627–631.
[4] J. Wittbrodt, A. Shima, M. Schartl, Medaka – a model organism from the far East, Nat. Rev. Genet. 3 (2002) 53–64.
[5] H. Zhao, J. Duan, N. Cheng, Y. Nagahama, Specific expression of Olpiwi1 and Olpiwi2 in medaka (*Oryzias latipes*) germ cells, Biochem. Biophys. Res. Commun. 418 (2012) 592–597.
[6] T. Iwamatsu, Stages of normal development in the medaka *Oryzias latipes*, Mech. Dev. 121 (2004) 605–618.
[7] J.C. Gilkey, Roles of calcium and pH in activation of eggs of the medaka fish *Oryzias latipes*, J. Cell Biol. 97 (1983) 669–678.
[8] S.E. Webb, R.A. Fluck, A.L. Miller, Calcium signaling during the early development of medaka and zebrafish, Biochimie 93 (2011) 2112–2125.
[9] R. Nuccitelli, The electrical changes accompanying fertilization and cortical vesicle secretion in the medaka egg, Dev. Biol. 76 (1980) 483–498.
[10] K. Asami, A. Irimajiri, T. Hanai, Development of medaka eggs as monitored by their dielectric behavior, Bull. Inst. Chem. Res. Kyoto Univ. 64 (1987) 339–343.
[11] J. Gimsa, T. Müller, T. Schnelle, G. Fuhr, Dielectric spectroscopy of single human erythrocytes at physiological ionic strength: dispersion of the cytoplasm, Biophys. J. 71 (1996) 495–506.
[12] R. Pethig, Review article – dielectrophoresis: status of the technology theory and applications, Biomicrofluidics 4 (2010).
[13] V.L. Sukhorukov, R. Reuss, J.M. Endter, S. Fehrmann, A. Katsen-Globa, P. Gessner, et al., A biophysical approach to the optimisation of dendritic–tumour cell electrofusion, Biochem. Biophys. Res. Commun. 346 (2006) 829–839.
[14] M. Sancho, G. Martínez, S. Muñoz, J.L. Sebastián, R. Pethig, Interaction between cells in dielectrophoresis and electrorotation experiments, Biomicrofluidics 4 (2010).
[15] D. Zimmermann, A. Zhou, M. Kiesel, K. Feldbauer, U. Terpitz, W. Haase, et al., Effects on capacitance by overexpression of membrane proteins, Biochem. Biophys. Res. Commun. 369 (2008) 1022–1026.
[16] G. Fuhr, U. Zimmermann, S.G. Shirley, Cell motion in time-varying fields: principles and potential, in: U. Zimmermann, G.A. Neil (Eds.), Electromanipulation of Cells, CRC Press Inc., Boca Raton, 1996, pp. 259–328.
[17] T.B. Jones, Electromechanics of Particles, Cambridge University Press, 2005.
[18] W. Arnold, U. Zimmermann, Electro-rotation – development of a technique for dielectric measurements on individual cells and particles, J. Electrost. 21 (1988) 151–191.
[19] K.L. Chan, H. Morgan, E. Morgan, I.T. Cameron, M.R. Thomas, Measurements of the dielectric properties of peripheral blood mononuclear cells and trophoblast cells using AC electrokinetic techniques, Biochim. Biophys. Acta 1500 (2000) 313–322.
[20] V.L. Sukhorukov, J.M. Endter, D. Zimmermann, R. Shirakashi, S. Fehrmann, M. Kiesel, et al., Mechanisms of electrically mediated cytosolic Ca^{2+} transients in aequorin-transformed tobacco cells, Biophys. J. 93 (2007) 3324–3337.
[21] G. Abou-Ali, K.V.I.S. Kaler, R. Paul, N.K. Björklund, R. Gordon, Electro rotation of axolotl embryos, Bioelectromagnetics 23 (2002) 214–223.
[22] N.H. Hart, R. Pietri, M. Donovan, The structure of the chorion and associated surface filaments in Oryzias—evidence for the presence of extracellular tubules, J. Exp. Zool. 230 (1984) 273–296.
[23] U. Lei, P.-H. Sun, R. Pethig, Refinement of the theory for extracting cell dielectric properties from dielectrophoresis and electrorotation experiments, Biomicrofluidics 5 (2011) 44109–44116.
[24] R. Pethig, D.B. Kell, The passive electrical properties of biological systems: their significance in physiology, biophysics and biotechnology, Phys. Med. Biol. 32 (1987) 933–970.
[25] T. Iwamatsu, T. Muramatsu, H. Kobayashi, Oil droplets and yolk spheres during development of medaka embryos, Ichthyol. Res. 55 (2008) 344–348.